Int. J. Solids Structures Vol. 18, No. 12, pp. 1129–1144, 1982
Printed in Great Britain.

0020-7683/82/121129-16$03.00/0

A NEW EXPERIMENTAL METHOD IN DETERMINING CRACK PROPAGATION TRANSITION TEMPERATURE IN STEEL

P. LIPIŃSKI†
Department of Engineering, Metz University, Ile du Saulcy, 5700 Metz, France

and

J. R. KLEPACZKO†
Division of Engineering Brown University, Providence, RI 02912, U.S.A.

(*Received* 20 *July* 1981; *in revised form* 15 *March* 1982)

Abstract—This study concentrates on a new experimental method for determining propagation transition temperature (PTT) in carbon steel (0.45% C). The method is based on the Hopkinson bar concept, by which the nature of pressure-time relationship can be studied when a pulse is applied at the active end of the bar. This concept enables one to determine terminal crack velocity using the round tensile specimen of a proper geometry with the *V*-notch at the half of its length; the total speimen length is 900 mm. When such a specimen is pulled in a testing machine, the fracture occurs at the notch cross section. The fracture event produces elastic waves which can be analyzed, and thus, the crack velocity can be estimated. This technique has been applied in several temperatures to monitor crack velocity changes. The analysis of oscillograms indicated a sharp change in the average crack velocity as well as in the average acceleration within a very narrow range of temperatures. It has been observed that the propagation transition temperature occurs within the limits $\Delta T \approx 10$ K, and for steel 0.45%C PPT ≈ 252 K.

1. INTRODUCTION

Many researchers have focussed their attention on the problems of crack dynamics in the past decade. During this period some new experimental techniques have been introduced to measure crack initiation under dynamic conditions of loading[1, 2]. Dynamic crack propagation and arrest was also studied with a variety of new experimental techniques. The most accepted technique for this purpose is a wedge loaded rectangular double cantilever beam specimen (DCB) combined with the grid resistance gage to monitor crack velocity[3–5, 36, 37], or with an optical method to measure both crack velocity and stress intensity factor for the running crack, for example [6–10]. Dynamic theoretical analyses of crack propagation and arrest in a wedge loaded rectangular DCB specimen have revealed the complexity of the mechanics of this specimen [3, 9, 11, 12].

The results obtained with these experimental techniques demonstrate that dynamic crack propagation for a particular material can be described at a constant temperature by a univalued relation between fracture resistance K_{ID} and crack velocity v_c. This relation $K_{ID}(v_c)_T$, where K_{ID} is the fracture resistance of a running crack, and v_c is the crack velocity, has been obtained experimentally for plastics as well as for metallic materials, for example [7, 8, 13–16].

In the case of brittle metallic materials, including steel, the $K_{ID}(v_c)_T$ relation has the characteristic shape which is shown schematically in Fig. 1. In the case of lower crack velocities (for a brittle steel up to 400 ms^{-1}) the fracture resistance K_{ID} remains almost constant or indicates a small minimum, but at higher velocities K_{ID} increases sharply reaching a very high value at the crack velocity which may be recognized as an asymptotic value v_∞.

Theoretical studies on fast crack propagation in elastic bodies indicate that for a non-driven crack, when only the natural inertia forces are present, crack velocity may attain a very high fraction of the elastic wave speed[17–29]. For example Mott[7], Craggs[21], and later Berkvist[22] have shown that the limiting speed for an elastic crack tip is

$$v_c \approx 0.38C_1 \quad \text{or} \quad v_c \approx 0.6C_2$$

†On leave from the Institute of Fundamental Technological Research, Warsaw, Poland.

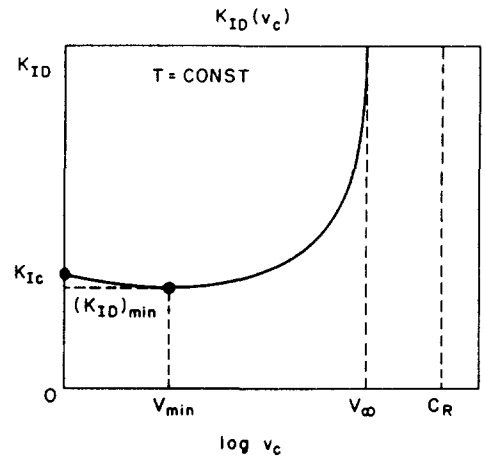

Fig. 1. Possible curve of fracture resistance vs crack velocity $K_{ID}(v_c)$ for brittle metallic alloys (steels); K_{Ic}–fracture toughness at quasi-static initiation; v_∞–terminal crack velocity, C_R–Rayleigh wave speed.

where C_1 is the speed of the longitudinal pressure wave (p-wave) and C_2 is the speed of elastic shear wave (s-wave). The value of C_2 is approximately equal to the surface elastic wave speed C_R (Rayleigh wave speed). Also Broberg[19] derived a similar relation between v_c and C_R. Further theoretical and experimental studies have shown that the terminal crack velocity depends on many factors like specimen size, temperature, ductility and others[3–12, 25–29]. The terminal crack velocity depends generally on the boundary values. Experimental results demonstrate conclusively that the maximum crack speed observed in practice is considerably lower than the speed of Rayleigh waves. Since the energy dissipation per unit of crack extension is extremely sensitive to the crack tip velocity in the high velocity range, a small plastic deformation at the crack tip and within the process zone may contribute substantially towards limiting of the terminal velocity. Thus, due to dissipative processes in the vicinity of the crack tip and due to inertia effects the terminal crack velocity is effectively limited to a small fraction of the Rayleigh wave speed[30]. One of the most probable key factors, besides inertia effects, which limits the velocity of ductile cracks in metals and alloys is a very high strain rate sensitivity observed within the high strain rate region $10^3\,s^{-1} \leq \dot{\epsilon} \leq 10^6\,s^{-1}$, see for example[31].

In conclusion, an exact experimental measurement of the terminal velocity under different conditions, for example at different temperatures, or for different materials, can provide additional information on crack propagation dynamics.

2. PROPAGATION TRANSITION TEMPERATURE

It is well known that mechanical properties of BCC metals and their alloys, like the maximum tensile deformation, the fracture energy measured from the Charpy test and the fracture toughness of crack initiation, depend strongly on temperature. Many types of laboratory tests have been proposed with this in mind. However, a very limited number of experimental methods, and in consequence experimental results, have been concerned with fracture propagation as a function of temperature. The most important single result of the fracture propagation research reported in the literature is the finding that an abrupt change in fracture propagation characteristics occurs for steels at some transition temperature[32, 33]. It has been observed during a full-scale experiment with pressurized pipes that the crack velocity undergoes a sharp transition at a particular temperature. This temperature is called the propagation transition temperature (PTT). Above this temperature the terminal crack velocity v_c is much lower and the appearance of the fractured surfaces is fibrous. Below the PTT the fracture appearance is cleavage and the terminal crack velocity is much higher. For example, full-scale experiments on two different pipe steels described in [33] have revealed the following values: steel "*FF*", PTT denoted as T_p, $T_p \approx 292$ K; crack speed at temperatures higher than T_p is $v_{cL} \approx 0.137$ mm/μs, and crack speed at temperatures lower than T_p is $v_{cH} = 0.507$ mm/μs;

the respective values for steel "M" are $T_p \approx 262$ K, $v_{cL} \approx 0.179$ mm/μs, and $v_{cH} \approx 0.656$ mm/μs. Thus, the speed plateaus have been observed for both materials. The transition region is usually very narrow, and is limited to 10 K.

Mostly, an attempt to estimate the PTT in the laboratory focusses on an indirect method such as measurement of transition temperatures of crack initiation on CVN or DWTT (Charpy V-notch; Drop-Weight Tear Test),[32]. These indirect methods, though sometimes successful, cannot fully reflect the complicated nature of propagating crack. A more appropriate laboratory method to measure the PTT utilizes a grid resistance gage cemented across the expected crack path in the DCB specimen which is then placed in a low temperature chamber[5, 36, 37]. But it is known that because of the interaction of elastic waves emitted from the moving crack inside such a specimen, and because conditions of crack initiation frequently differ depending on the bluntness of notch, the maximum crack velocity may vary. The DCB method seems to complicate the laboratory measurement of the PTT and demands a proper interpretation of experimental data.

The purpose of this paper is to give an account of a method which enables the measurement of the terminal crack velocity. The applicability of this method was demonstrated in [30], where the terminal velocities of crack propagation have been measured at room temperature for two aluminum alloys.

3. THE EXPERIMENTAL METHOD

The technique is based on the Hopkinson bar concept where the nature of pressure-time relationship can be studied when a pulse is applied at the active end of the bar. The original idea of the instrumented Hopkinson bar is due to Davies[34]. A long bar made of a hard steel was used to measure precisely the pressure pulse $p(t)$ of a short duration developed by an event at the impact end. Assuming that the Hopkinson bar remains always elastic, the pulse is transmitted along the bar with the elastic wave speed C_0, and is recorded by a capacitance gage at the free end of the bar. The principles of this technique are given frequently in the literature[34, 35].

The basic concept of the Hopkinson bar remains essentially the same, the only exception being the more prevalent use of resistance strain gages cemented on the bar surface. Thus, the elastic strain-time history $\epsilon(t)$ rather than the elastic displacement-time history $U(t)$ is obtained. The displacement can be calculated from the relation

$$U(t) = C_0 \int_0^{\theta} \epsilon(t)\, dt \tag{1}$$

where $\epsilon(t)$ is the elastic strain-time history measured by the resistance gage, and C_0 denotes the elastic wave speed. In addition the stress pulse in the bar can be calculated using Hook's law

$$\sigma(t) = \rho_0 C_0^2 \epsilon(t), \quad E = \rho_0 C_0^2 \tag{2}$$

where ρ_0 is the density and E is Young modulus. The duration of the longitudinal pulse is denoted by θ, the wave length is then $\lambda = C_0\theta$.

The fundamental assumption of this technique is that longitudinal waves in the bar propagate without dispersion. Some analyses have shown that this is true only for the waves approximately longer than $\lambda_m \approx 5D$[35], where D denotes diameter of the measuring bar.

A factor of great importance is that when the impact end of the bar is loaded non-symmetrically with respect to the axis, both longitudinal and flexural waves are set-up. The Rayleigh approximation[35] of the flexural wave speed C^* shows the general dependence on the wavelength λ. Since C^* depends on λ, a flexural disturbance of an arbitrary shape will not propagate along a bar without dispersion. In addition, the speed of flexural waves C^* is much lower than the speed of longitudinal waves C_0. For short flexural waves which travel faster than longer ones the limiting speed is $C^*_{max} \approx 0.6C_0$.

If the Hopkinson bar is loaded at the impact end by a nonaxial force of duration θ, then two waves will be emitted. Since the bending wave is much slower, at a specific distance X_{min} these

waves will be completely separated, and one gage can monitor both waves in a consecutive time intervals. To obtain X_{min} the following condition holds

$$X_{min}\left(\frac{1}{C_0}-\frac{1}{C^*_{max}}\right)=\theta \tag{3}$$

and

$$X_{min}=\frac{C_0\theta}{1-\dfrac{C_0}{C^*_{max}}} \quad \text{or} \quad X_{min}=\frac{\lambda_0}{1-\dfrac{C_0}{C^*_{max}}} \tag{4}$$

where $\lambda_0 = C_0\theta$ is the length of longitudinal wave. Since $C_0/C^*_{max} = 0.5764$, $X_{min} = 2.361\lambda_0$ or

$$X_{min} = 2.361 C_0\theta. \tag{5}$$

For example, assuming $\theta = 10\,\mu$s and $C_0 = 5$ mm/μs the expression (5) gives $X_{min} = 118$ mm. A more exact discussion of eqn (5) can be found in [30].

In order to measure crack velocity a special specimen arrangement has been proposed. The round tensile specimen with the V-notch at the half length is applied as shown schematically in Fig. 2. The specimen is relatively long to avoid immediate wave reflections from the grip ends. The V-notch radius is kept as small as possible to develop a large enough stress gradient at the crack initiation.

When the NRTL specimen (notched round tensile long) is pulled slowly in a universal testing machine, a fracture occurs at the maximum load and cracking starts to develop. Next, the crack starts to propagate with a high velocity through the notched cross section. As a result fracture event produces two elastic pulses which propagate symmetrically in opposite directions away from the notch. The elastic longitudinal unloading wave $\epsilon^-(t)$ and a group of bending waves $C^*(t)$ are emitted. The NRTL specimen is long enough to avoid reflections, so both pulses can be measured undisturbed. The duration of these waves is equal to the time of fracturing, and the shape of both waves depends on the fracture process. The phase diagram for the longitudinal unloading wave is shown in the upper part of Fig. 2. The NRTL specimen has two gage stations. Gage 1, placed near the notch, triggers the electronic recording equipment, whereas station 2 consists of two very short SR gages (gage length 2 mm) cemented on opposite

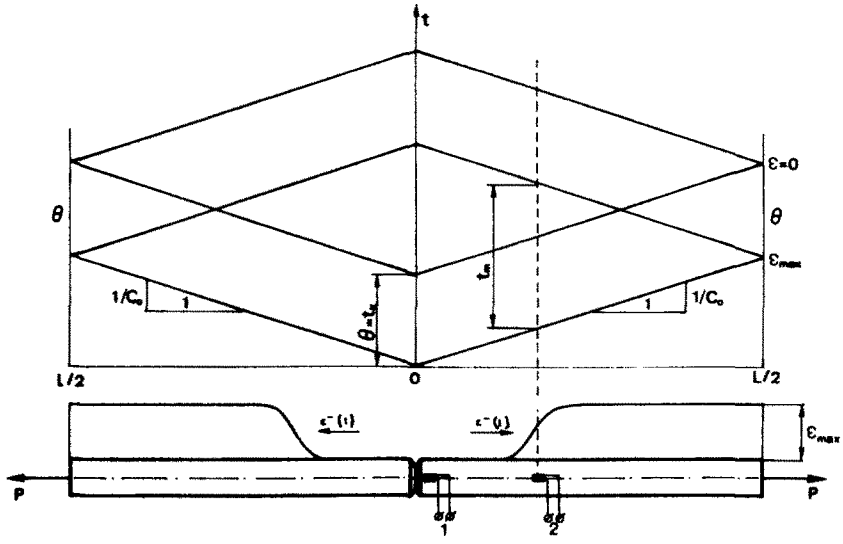

Fig. 2. Specimen configuration and the phase diagram; 1 – triggering gage, 2 – measuring gage; $\epsilon^-(t)$ – unloading elastic wave; t_k – fracture time; t_m – maximal time of measurement.

sides of the bar. Measuring station 2 is placed at the distance X_g from the loading end which is larger than X_{min} calculated from eqn (5). Since the gages are connected in series, station 2 enables to monitor only the unloading longitudinal wave. As it will be shown later, this information is sufficient to estimate changes in the crack velocity. Since the NRTL specimen is long enough, there exists a time interval t_m (as shown in Fig. 2) during which the recording can be completed without any interference. Signals from both stations are transmitted through an amplifier to the triggering input (gage 1) and to the $y(t)$ input of an oscilloscope (gage 2). The signal from the measuring station is recorded as a function of time with the aid of a Polaroid camera or transient recorder.

A universal testing machine loading the NRTL specimen in tension enables one to record the initial portion of the force-time $P^+(t)$ or force-displacement $P^+(\Delta l)$ diagram. This procedure provides a calibration of the dynamic part of the test since the unloading waves begin from the maximum elastic strain ϵ_{max} which can be calculated from the $P_{max}(t)$ or $P^+(\Delta l)$ records obtained with the machine chart recorder. This procedure is based on Hooke's law and the notch diameter must be small enough not to yield any outside portion of the specimen.

It is also possible to load the NRTL specimen with a prefatigued crack dynamically from one end by a rapidly rising tensile pulse resulting from the detonation of explosives. This experimental procedure was applied in [1, 38] for evaluation of the dynamic fracture initiation properties of steels. In this way a very high loading rate $\dot{K}_I$ may be obtained, in excess of $10^6\,\mathrm{MPa}\sqrt{\mathrm{m}}\,\mathrm{s}^{-1}$.

A long glass rod with a side scratch was used in [39, 40] to study the dynamics of brittle fracture. Those glass rods were pulled slowly at a constant cross-head velocity to fracture and the shape of the pulses induced by the facture was measured by means of strain gages. It was found that the shapes of the unloading pulses could be accurately predicted by the theory of elastic waves [39].

The longitudinal pulses produced by fracture in a hard metal wire loaded in tension were also studied experimentally in [41]. This study was connected with the question of the frequency response of strain gages.

One of the earliest papers on the brittle fracture of a rod specimen [42] has shown that in some tensile tests on brittle steel and PMMA elastic waves, both symmetric and anti-symmetric, are emitted from the fracturing zone.

All the papers discussed above demonstrate that application of the Hopkinson bar concept to fracture dynamics is an effective method in many experimental configurations.

4. EXPERIMENTS

The present investigation was undertaken to study the effect of temperature on the terminal crack velocity in steel. For this purpose the NRTL specimen has been used. Such a specimen instrumented with strain gages could be easily placed into a low temperature chamber and slowly pulled in a universal testing machine. A series of tests were performed at several temperatures below room temperature. All NRTL specimens wer made of 0.45%C carbon steel with the following dimensions: total length $L = 900$ mm, bar diameter $D = 12$ mm, V-notch 45°, notch radius $\sim 30\,\mu$m. Two notch diameters were used to control crack speed more exactly, $d = 5$ mm and $d = 7.8$ mm. Experiments were performed at five temperatures: $T = 200$, 230, 250, 270 and 295 K. For each temperature two or three tests were conducted. For each test the record of initial loading $P^+(\Delta L)$ plus oscillogram $\epsilon^-(t)$ has been obtained. In addition to the testing machine chart recorder the quasi-static portion of the test was measured with a Peters LVDT extensometer [14, 43] with pins attached 50 mm apart. The notch was exactly in the center of the 50 mm gage length. Thus, each test provided three records $P^+(t)$, $P^+(\Delta L)$ and $\epsilon^-(t)$. The measuring station 2 was situated at the distance $X_g = 120$ mm (10D) from the notch. The applied geometry made possible to obtain the maximum time of measurement without any interference $t_m = 90\,\mu$s.

All oscillograms were measured using a digital measuring microscope and the numerical data were thus obtained to plot $P^-(t)$, i.e. the force which is acting on the notch cross section during the process of fracture. Fig. 3 shows two measured oscillograms in the form $P^-(t)$ for two specimens with $d = 7.8$ mm tested at 295 and 200 K. These plots give directly the fracture time t_k at 295 K, $t_k = 9.6\,\mu$s and at 200 K, $t_k = 8.7\,\mu$s. As a next step before comparing the

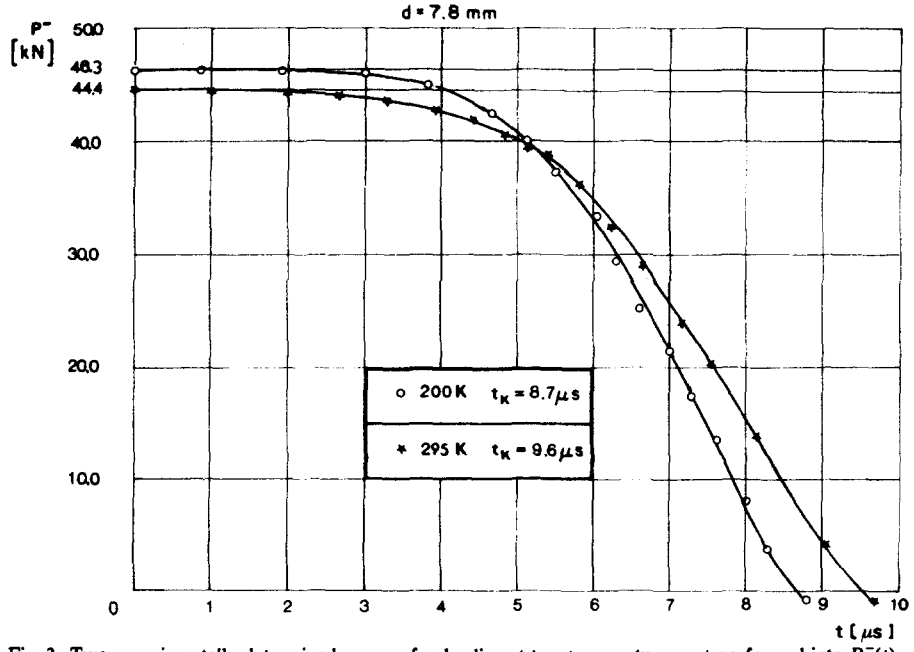

Fig. 3. Two experimentally determined waves of unloading at two temperatures as transformed into $P^-(t)$, P denotes force in the bar; notch diameter d = 7.8 mm.

results with theoretical analysis, all experimental results were replotted in non-dimensional coordinates: non-dimensional force ξ and non-dimensional time τ

$$\xi = \frac{P^-}{P_{max}} \quad \text{and} \quad \tau = \frac{t}{t_k}. \tag{6}$$

Thus, the non-dimensional experimental diagrams $\xi(\tau)$ can be constructed. One of these plots obtained for 200 K and for notch diameter $d = 5$ mm is shown in Fig. 4. The experimental points

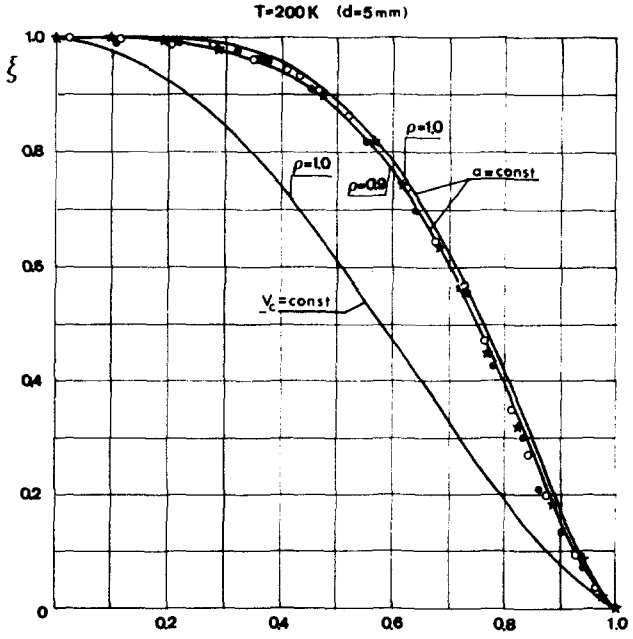

Fig. 4. Non-dimensional plot of $\xi(\tau)$, ξ-non-dimensional force, τ-non-dimensional time, notch diameter $d = 5$ mm. Solid lines are predicted theoretically.

shown for three specimens demonstrate a remarkably small scatter. All experimental data confirmed the high repeatability of tests conducted under the same conditions. The very small scatter made possible a more exact quantitative analysis of experimental data.

5. SHAPES OF THE UNLOADING WAVE

The shape of the unloading wave is directly related to the fracture kinetics at the notch cross section. The investigation which was carried out in [39], where circular glass rods with a side scratch were subjected to simple extension, demonstrated that tthe shapes of both longitudinal and flexural pulses could be accurately predicted. Theoretical predictions of these pulses were exact enough when it was assumed that the crack velocity is constant throughout the fracture process and that the stress distribution across the unbroken cross-section did not change. Under the assumption of constant crack velocity the three theoretical shapes of unloading wave can be predicted. When the crack originates at any point of the notch tip a through cross-section fracture is observed [39, 41]. For this case the relation $\xi(\tau)$ takes the form

$$\xi(\tau) = \left\{1 - \frac{1}{\pi}[4\tau^2 \cos^{-1}\tau + \cos^{-1}(1-2\tau^2) - 2\tau(1-\tau^2)^{1/2}]\right\} \quad 0 \le \tau \le 1. \tag{7}$$

When the fracture process is symmetrical about the bar axis a so called radial fracture occurs. In this event there are two possibilities, the first, when the separation starts simultaneously at many points around the notch tip and the crack front converges onto the rod axis, and the second, when the crack starts at the rod axis and propagates radially outward to the notch tip. The last case resembles the fracture mechanics in the neck. These two cases have been discussed elsewhere [30]. In the first case (crack starts around the notch)

$$\xi(\tau) = 1 - 2\tau + \tau^2 \quad 0 \le \tau \le 1. \tag{8}$$

In the second case (crack starts at the rod axis)

$$\xi(\tau) = 1 - \tau^2 \quad 0 \le \tau \le 1. \tag{9}$$

It has been observed that only eqns (7) and (9) predict shapes $\xi(\tau)$ which resemble oscillograms. The shape of the oscillogram predicted by eqn (8) has never been observed. Since there were still some discrepancies between the oscillograms and the shapes $\xi(\tau)$ offered by eqns (7) and (9) a more general case has been analyzed.

Let us assume that across a regular cross-section of a bar the crack front propagates with velocity $v_c(x, y, t)$. The origin of the fracture process is situated at the point characterized by the vector $\vec{r}_0$ (see Fig. 5). The actual tensile force carried by the bar is

$$P^-(t) = \int_{S(t)} \sigma_z(x, y, t)\, dS \tag{10}$$

where $\sigma_z(x, y, t)$ denotes the axial stress and $S(t)$ is the non-fractured area of the bar. The minus sign indicates the process of unloading. Thus, neglecting a small plastic zone along the crack front, the remaining parts of the bar undergo the dynamic process of elastic unloading. Applying Hooke's law, the pulse $\epsilon^-(t)$ which is measured as an elastic wave is proportional to $P^-(t)$. The following two assumptions have been made: the crack front is a circle or its part has a circular shape, and the axial stress is constant throughout the fracture process having an average value $\bar{\sigma}_z$

$$\bar{\sigma}_z(t) = \frac{1}{S(t)} \int_{S(t)} \sigma_z(x, y, t)\, dS; \quad \bar{\sigma}_z(t) = \text{const.} \tag{11}$$

To check the second assumption the finite element technique has been used to predict changes

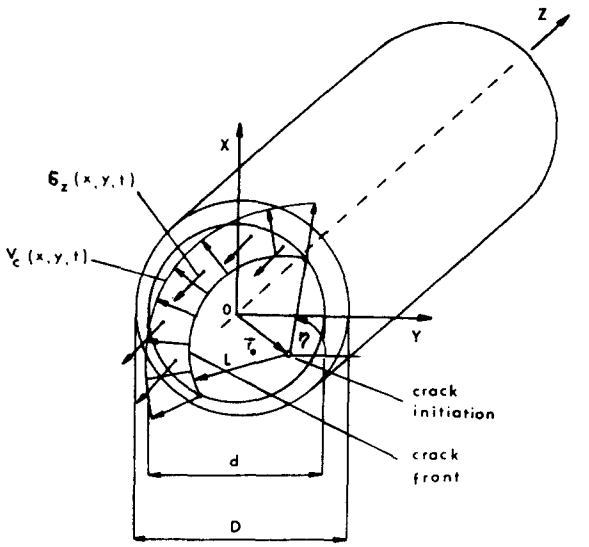

Fig. 5. General case of fracturing for a regular rod.

in the elastic–plastic stress and strain fields in the notched cross section of the bar. The calculations performed with the elastic–plastic model of material behavior taking into account the non-linear strain hardening revealed the validity of the second assumption[44]. A complete set of calculations was performed for two temperatures 200 and 295 K and for two notch cross-sections $d = 5.0$ and 7.8 mm using experimental stress–strain curves measured at these temperatures. The calculations were stopped at the same force at which a particular specimen broke. Distributions of normal stress $\sigma_z(x, y)$ at the instant of fracture showed the stress differences at the axis and at notch do not exceed an average ratio $(\sigma_{z0}/\sigma_{zr})_{200} = 0.761$ for 200 K, and $(\sigma_{z0}/\sigma_{zr})_{295} = 1.316$ for 295 K, where σ_{z0} and σ_{zr} are respectively the normal stresses at the axis and at the notch. These ratios are even smaller for $d = 5.0$ mm. If the maximum normal stress is responsible for the crack initiation then the numerical analyses demonstrate that the crack should start near the notch at low temperatures and near the axis at higher temperatures. This conclusion is completely consistent with experimental observations.

The direct consequence of the first assumption and axial symmetry is that in order to calculate the shape of the unloading wave only one factor must be known, namely the non-dimensional radius of crack initiation $\rho = r_0/r_m$, where r_0 is the radius of the point of crack initiation, and $r_m = d/2$ is the specimen radius at the notch. It has also been assumed that the variations of crack velocity can be approached by the series

$$v_c(t) = \bar{a}t_k \sum_{i=1}^{n} \alpha_i \tau^i \tag{12}$$

where $\bar{a}$ is an average acceleration, and τ is non-dimensional time as previously defined. If the origin of the coordinate system is assumed at the point of crack initiation, the actual position of the crack front after integration of (12) is

$$L = \bar{a}t_k \sum_{i=1}^{n} \frac{\alpha_i}{i+1} \tau^{i+1}. \tag{13}$$

For the case when $\rho \neq 0$, i.e. for non-axial fracture, two fracture periods occur. The first, from the beginning of initiation to the moment when the nearest point of notch tip is reached $(0 \leq t \leq t_s)$. The second one follows the first and lasts until the the fracture is complete and both specimen parts are separated $(t_s \leq t \leq t_k)$. The decrement of the axial force due to crack advancement is

$$-\mathrm{d}P = \tilde{\sigma}_z r \, \mathrm{d}r \, \mathrm{d}\eta. \tag{14}$$

During the first period the relation (14) has the form

$$-\mathrm{d}P = 2\pi\bar{\sigma}_z r\,\mathrm{d}r. \tag{15}$$

Taking into account eqn (13) in eqn (15) and integrating with the initial conditions $t = 0$ and $P = P_{max}$, the non-dimensional force during the first period is

$$\xi(\tau, \rho) = 1 - 4\tau^2(1+\rho)^2\left(\sum_{i=1}^{n}\frac{\alpha_i}{i+1}\tau^i\right)^2 \tag{16}$$

This is true for $0 \le \tau \le \tau_s$.

The second period can be described by analogy integrating eqn (14) within the following limits

$$\eta = \pm\cos^{-1}\left(\frac{2r^2 + 2\rho^2 r_s^2 - r_s^2}{2\rho r r_s}\right)$$

$$r = \begin{cases} r_m[(1-\rho^2\sin^2\eta)^{1/2} + \rho\cos\eta] \\ r(t) \end{cases}.$$

The angle η defines the interaction of the crack front with the notch tip (see Fig. 5).

Thus, the non-dimensional force $\xi(\tau, \rho)$ during the second period is

$$\xi(\tau, \sigma) = \begin{cases} 1 - \frac{1}{\pi}\cos^{-1}\dfrac{\rho - 4(1+\rho)^2\left(\sum\frac{\alpha_i}{i+1}\tau^{i+1}\right)^2 + 1}{2\rho} + \\ -\dfrac{4(1+\rho)^2\left(\sum\frac{\alpha_i}{i+1}\tau^{i+1}\right)^2}{\pi}\cos^{-1}\left[\rho^2 - 1 + 4(1+\rho)^2\left(\sum\frac{\alpha_i}{i+1}\tau^{i+1}\right)^2\right] + \\ +\dfrac{1}{2\pi}\left\{4\rho^2 - \left[1 + \rho^2 - 4(\rho+1)^2\left(\sum\frac{\alpha_i}{i+1}\tau^{i+1}\right)^2\right]^2\right\}^{1/2}. \\ \tau_s \le \tau \le \tau_k. \end{cases} \tag{17}$$

The time τ_s can be calculated from the following relation

$$\frac{1-\rho}{1+\rho} = 2\sum_{i=1}^{n}\frac{\alpha_i}{i+1}\tau_s^{i+1}. \tag{18}$$

Equations (16)–(18) specify the whole fracture process. In these equations the non-dimensional radius of fracture initiation ρ enters as a parameter. Shapes of unloading waves calculated in the coordinates (ξ, τ) under the assumption of constant crack velocity are shown for different values of ρ in Figs. 6 and 7. For this case the velocity function (12) takes the form

$$v_c(t) = \bar{a}t_k\alpha_0. \tag{19}$$

Coefficient α_0 is determined from the condition $\tau = 1$ for $\xi = 0$, it gives $\alpha_0 = 1/2$.

Shapes of unloading waves for the case of constant crack acceleration are shown in Figs. 8 and 9. The velocity (12) has the form

$$v_c(t) = \bar{a}t_k\alpha_1\tau \tag{20}$$

for this case $\alpha_1 = 1$.

For the general case when crack velocity varies as a function of time the coefficients α_i in eqn (12) are determined by comparison with experimental data.

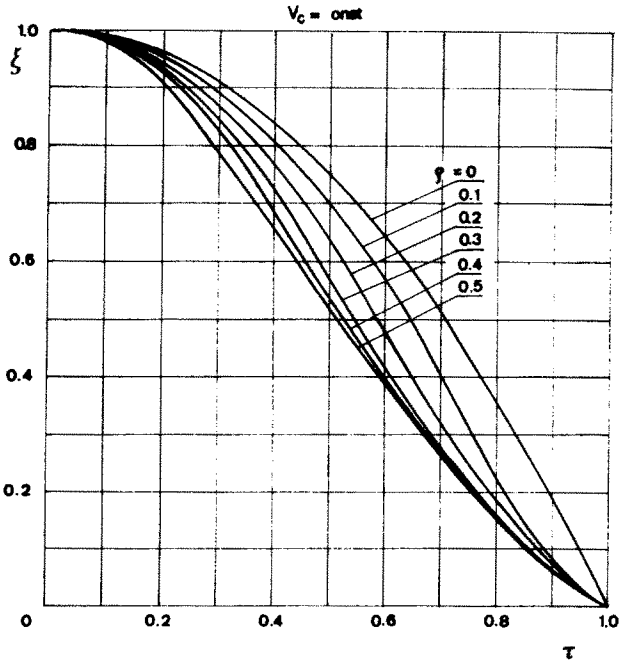

Fig. 6. Calculated shapes of the unloading elastic wave for different values of the non-dimensional radius of fracture initiation ρ, $0 \leq \rho \leq 0.5$; v_c = const.

6. EXPERIMENTAL RESULTS

As has been mentioned previously, all oscillograms were transformed after digitizing into (ξ, τ) coordinates. Since the non-dimensional radius of fracture initiation ρ enters as a parameter in all of the derived equations, the criterion for comparison with experimental data has been chosen in the form to fit the entire calculated shape of the wave profile for both $\bar{v}_c$ = const and $\bar{a}$ = const at a particular value of ρ. The result of such comparison is shown in Fig. 4 (T = 200 K, d = 5 mm). The three solid lines indicate calculated values, the lowest curve

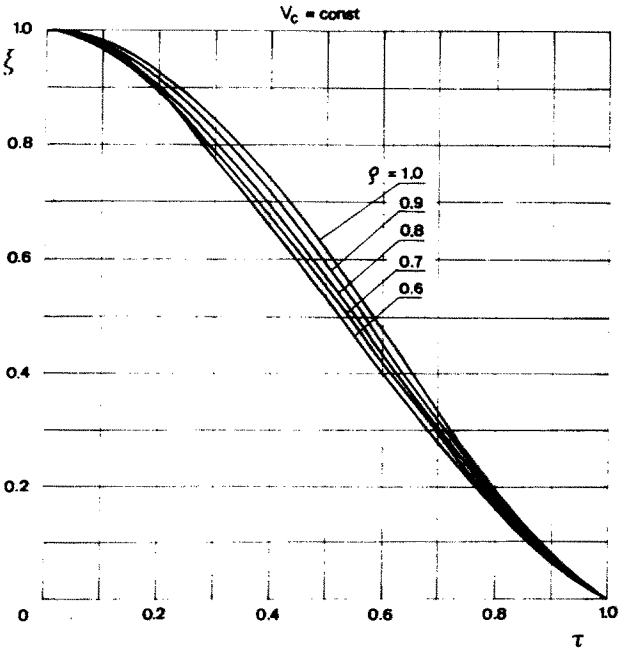

Fig. 7. Calculated shapes of the unloading elastic wave for different values of the non-dimensional radius of fracture initiation ρ, $0.5 \leq \rho \leq 1.0$; v_c = const.

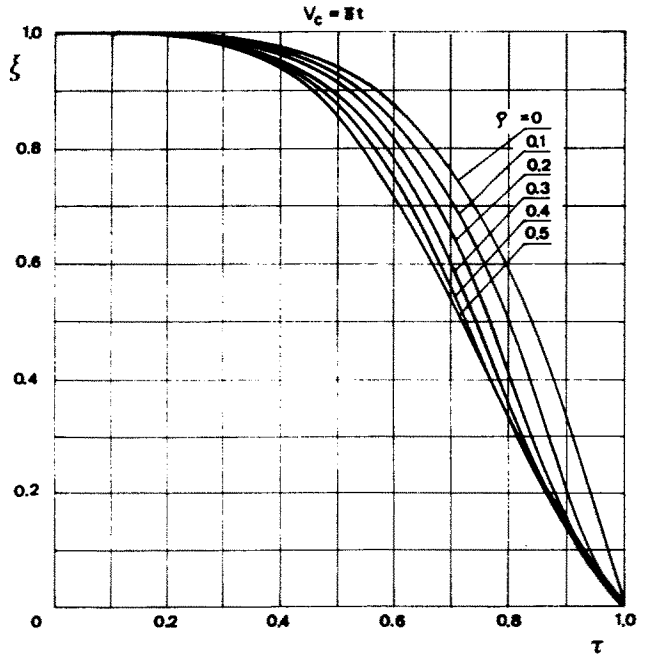

Fig. 8. Calculated shapes of the unloading elastic wave for different values of the non-dimensional radius of fracture initiation ρ, $0 \leq \rho \leq 0.5$, a = const.

is obtained under the assumption of constant crack velocity v_c and $\rho = 1$, the two upper curves refer to the constant acceleration a, respectively for $\rho = 1$ and $\rho = 0.9$. The best fit to experimental points which are measured from three tests is obtained for a = const and $\rho = 0.9$. This procedure was repeated for all experimental data at different temperatures. The first conclusion is that the best fit is always observed for constant acceleration a. The discrepancy between experimental points and calculated profiles was so small that is was possible to

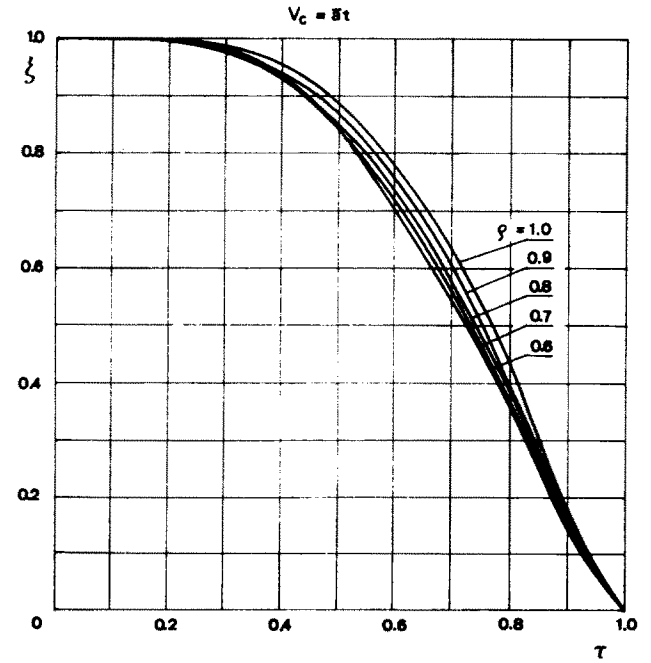

Fig. 9. Calculated shapes of the unloading elastic wave for different values of the non-dimensional radius of fracture initiation ρ, $0.5 \leq \rho \leq 1$, a = const.

estimate values of the non-dimensional radius of crack initiation for each test. The result is shown in Fig. 10. The further conclusion is that in fact only two cases of fracture have been observed. At lower temperatures through-cross section fracture is present, whereas at higher temperatures the radial fracture dominates with $\rho \approx 0$. This observation is in complete agreement with the previous study on aluminum alloys[30] as well as with the finite element calculations. As mentioned previously, the results of finite element calculations indicate that at low temperatures the highest normal stresses are expected near the notch tip. At room temperature the highest normal stress was found at the specimen axis. These observations are referred to the normal stress fields just before fracture. The temperature at which this transition takes place depends on the notch geometry.

Having determined ρ and knowing the fracture time t_k an average acceleration $\bar{a}$ and an average crack velocity $\bar{v}_c$ can be calculated

$$\bar{a} = \frac{2(1+\rho)}{t_k^2} r_m \quad r_m = d/2 \tag{21a}$$

$$\bar{v}_c = \frac{1+\rho}{t_k} r_m. \tag{21b}$$

The results of these calculations for $\bar{a}(T)$ are shown in Fig. 11. The average crack velocity $\bar{v}_c$ as a function of temperature is shown in Fig. 12. Both figures indicate a sharp change in $\bar{a}$ and $\bar{v}_c$ within a very narrow range of temperatures. This is the propagation transition temperature. The transition occurs within the limits $\Delta T \approx 10$ K for both $\bar{a}(T)$ and $\bar{v}_c(T)$. Thus, the propagation transition temperature for the carbon steel (0.45% C) tested is:

$$T_p = 252 \pm 3 \text{ K}.$$

Since the constant acceleration is recognized as a good approximation, experimental points obtained for the notch cross sections 7.8 mm as well as 5.0 mm fit the same level for both shelves, the upper one for low temperatures $\bar{a}_L \approx 0.15$ mm/μs^2, and the lower one for temperature higher than PTT, $\bar{a}_H \approx 0.085$ mm/μs^2. Of course, crack velocity plateaus differ

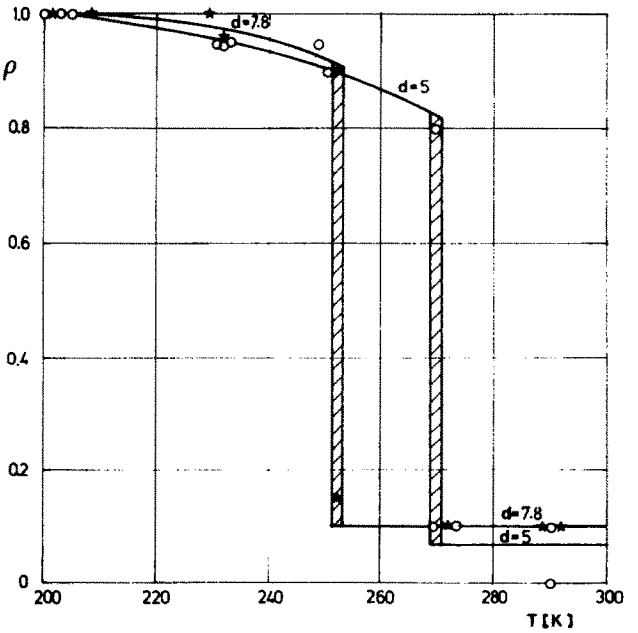

Fig. 10. Experimentally determined non-dimensional radius of crack initiation ρ as a function of test temperature, steel 0.45% C.

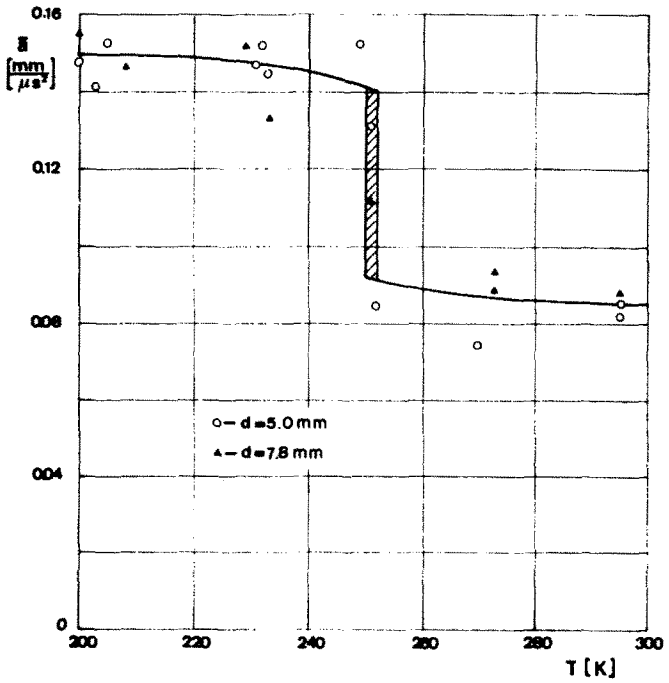

Fig. 11. Average crack acceleration $\bar{a}$ as a function of temperature.

depending on the notch diameter. For the upper shelf the values of crack velocity are: $\bar{v}_{cL} \approx 0.6\,\text{mm}/\mu\text{s}$ and $\bar{v}_{cL} \approx 0.75\,\text{mm}/\mu\text{s}$, respectively for $d = 5.0\,\text{mm}$ and $d = 7.8\,\text{mm}$, whereas for the lower shelf $\bar{v}_{cH} \approx 0.34\,\text{mm}/\mu\text{s}$ and $\bar{v}_{cH} \approx 0.45\,\text{mm}/\mu\text{s}$, respectively for $d = 5.0\,\text{mm}$ and $d = 7.8\,\text{mm}$. These values of $\bar{v}_c$ are higher than those obtained in [32, 33] especially for the lower shelf. A complete comparison of experimental data obtained during the course of the present investigation with those obtained in [32, 33] during the full scale experiments on pipes

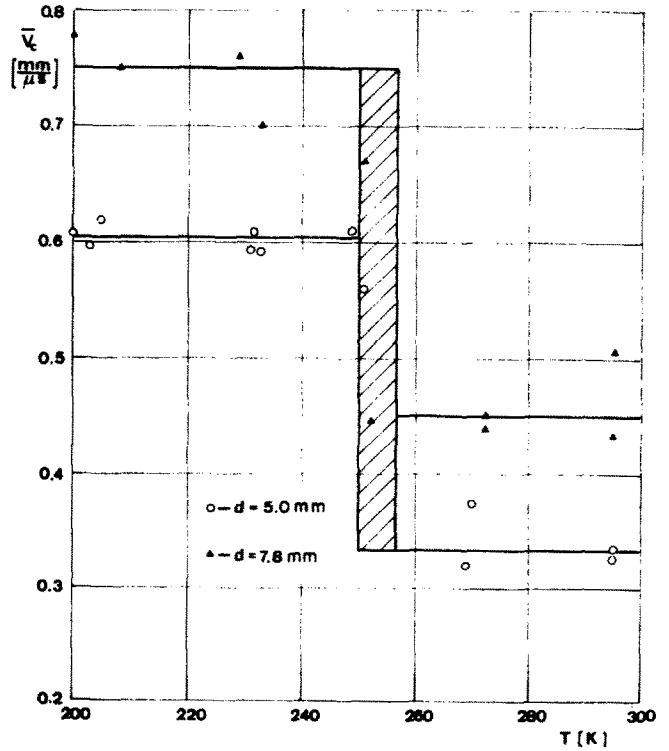

Fig. 12. Average crack velocity $\bar{v}_c$ as a function of temperature.

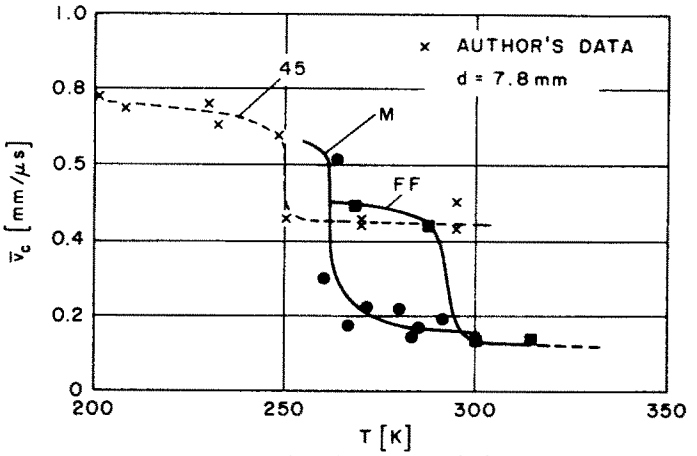

Fig. 13. Crack velocities measured as a function of temperature in full-scale experiments [32, 33], pipe steels *M* and *FF* heats, as compared with author's result $\bar{v}_c(T)$ for steel 45% C, broken line - denoted by 45, notch diameter $d = 7.8$ mm

are shown in Fig. 13. The entire shapes of the experimentally obtained functions $\bar{v}_c(T)$ are quite similar for all three cases. The broken line denoted as "45" indicates data from Fig. 12 for $d = 7.8$ mm. It may be thus concluded that the propagation transition temperature can be determined using the Hopkinson bar configuration, i.e. NRTL specimen.

7. DISCUSSION AND CONCLUSIONS

One implication of the nearly constant crack acceleration is that the propagating crack may reach the terminal velocity shortly before the specimen breaks. If it is assumed that the velocity function $v_c(\tau)$ is a third order polynomial, the terminal crack velocity v_{cm} can be calculated. Then the expression for $v_c(\tau)$ is

$$v_c(t) = \bar{a}t_k(\alpha_0 + \alpha_1\tau + \alpha_2\tau^2 + \alpha_3\tau^3) \tag{22}$$

and the four unknown coefficients α_i are related by equation

$$2\left(\alpha_0 + \frac{\alpha_1}{2} + \frac{\alpha_2}{3} + \frac{\alpha_3}{4}\right) = 1$$

which is the result of the condition that $\xi = 0$ for $\tau = 1$. Thus, only three coefficients α_i need to be determined. They have been obtained in such a way that the analytical curves $\xi(\tau)$ would fit most closely the shape of experimentally measured unloading waves. The result of these calculations for the notch diameter $d = 7.8$ mm is shown in Fig. 14. This figure indicates how crack velocity changes as a function of the nondimensional time τ. A very similar result has been obtained for the notch diameter $d = 5.0$ mm. Departure from constant acceleration is observed at the end of the crack travel when it slows down to its terminal velocity v_{cm}. At temperatures above PTT crack velocity reaches an almost constant value $(v_{cm})_H \approx 0.77$ mm/μs. At temperatures lower than PTT crack velocity is higher but even at $\tau \approx 1$ shows a tendency for a further increase; for this case $(v_{cm})_L \approx 1.31$ mm/μs. The Rayleigh wave speed for steel is about $C_R \approx 2.88$ mm/μs, and the ratios v_{cm}/C_R respectively are

$$\frac{(v_{cm})_H}{C_R} = 0.267 \quad \text{lower shelf } T \geq T_p$$

$$\frac{(v_{cm})_L}{C_R} = 0.455 \quad \text{higher shelf } T \leq T_p.$$

These values are still much lower than those predicted from the model of an ideal brittle solid,

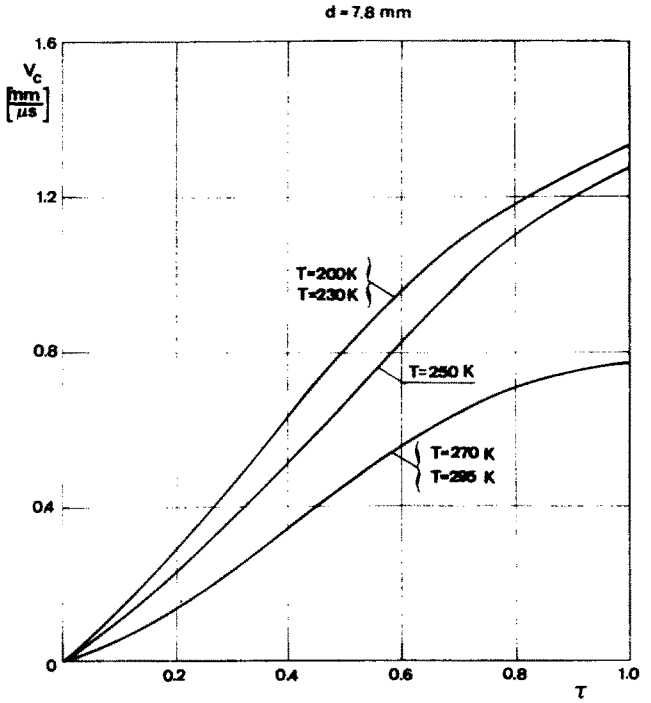

Fig. 14. Calculated values of crack velocity v_c as a function of non-dimensional time τ, notch diameter $d = 7.8$ mm.

i.e. $v_\infty/C_R \approx 0.6$. Since average accelerations for the lower and upper shelves are almost constant, the maximum crack velocities v_{cm} can be also estimated from the relation

$$v_{cm} = \sqrt{2\bar{a}d}. \tag{23}$$

For the notch diameter $d = 7.8$ mm, $\bar{a} = 0.085$ mm/μs^2 for $T \geq T_p$, and for $T \leq T_p$, $\bar{a} = 0.150$ mm/μs (see Fig. 11), eqn (23) predicts the following values of v_{cm}: $(v_{cm})_H = 1.15$ mm/μs and $(v_{cm})_L = 1.53$ mm/μs. As expected these values are in agreement with those obtained previously by an analysis of oscillograms. Though, calculated values from eqn (23) are overall higher.

Since the fracture resistance of running crack K_{ID} versus crack velocity v_c is believed to be a true material property the obtained values $(v_{cm})_H$ and $(v_{cm})_L$ should be localized on the $K_{ID}(v_c)$ diagram. For this purpose the numbers given above for v_{cm} have been compared with experimental data $K_{ID}(v_c)$ of Eftis and Krafft for a ship steel[13]. Values of v_{cm} for the upper and lower shelves from Figs. 12 and 13 fall in the proper portion of the $K_{ID}(v_c)$ plot in [13]. The value $(v_{cm})_L = 1.31$ mm/μs is almost equal to the asymptotic crack velocity v_∞ determined in [13].

It thus appears that the Hopkinson bar techique is a useful tool for obtaining certain parameters of crack dynamics. It is concluded that a sound methodology has been developed for determining the propagation transition temperature in metals and alloys. Still a comparison for exactly the same material should be performed between this laboratory technique and a full scale experiment.

REFERENCES

1. L. S. Costin, J. Duffy and L. B. Freund, Fracture initiation in metals under stress wave loading conditions. ASTM STP No. 627, ASTM (1977).
2. J. Klepaczko, Application of the split Hopkinson pressure bar to fracture dynamics. *Inst. Phys. Conf.* Ser. No. 47 (Edited by J. Harding). Oxford (1979).
3. M. F. Kanninen, C. Popelar and P. C. Gehlen, Dynamic analysis of crack propagation and arrest in the double-cantilever-beam specimen. ASTM STP No. 627, ASTM (1977).
4. J. F. Kalthoff, J. Beinert and S. Winkler, Measurements of dynamic stress intensity factors for fast running and arresting cracks in double-cantilever-beam specimens. ASTM STP No. 627, ASTM (1977).

5. D. A. Shockey, L. Seaman and D. R. Curran, Computation of crack propagation and arrest by simulating micro-fracturing at the crack tip. ASTM STP No. 627, ASTM (1977).
6. P. S. Theocaris and E. Katsamanis, Response of crack to impact by caustics. *Engng Fracture Mech.* **10**, 197 (1978).
7. L. Hodulak, A. S. Kobayashi and A. F. Emery, Influence of dynamic fracture toughness on dynamic crack propagation. *Engng Fracture Mech.* **13**, 85 (1980).
8. A. S. Kobayashi, Experimental-numerical stress analysis of a running crack. *Recent Research on Mechanical Behavior of Solids*. University of Tokyo Press, Tokyo (1979).
9. A. S. Kobayashi, A. F. Emery and S. Mall, Dynamic finite element and dynamic photoelastic analyses of two fracturing homalite-100 plates. Exp. Mech. **16**, 321 (1976).
10. A. J. Rosakis, Analysis of the optical method of caustics for dynamic crack propagation. *Engng Fracture Mech.* **13**, 331 (1980).
11. M. F. Kanninen, A dynamic analysis of unstable crack propagation and arrest in the DCB test specimen. *Int. J. Fracture* **10**, 415 (1974).
12. L. B. Freund, A simple model of the double cantilever beam crack propagation specimen. *J. Mech. Phys. Solids* **25**, 69 (1977).
13. J. Eftis and J. M. Krafft, A comparison of the initiation with the rapid propagation of a crack in a mild steel plate. *Trans. ASME Ser. D, J. Basic Engng* **87**, 275 (1965).
14. G. T. Hahn, R. G. Hoagland, and A. R. Rosenfield, Fast fracture toughness of steels. *Proc. Int. Conf. on Dynamic Fracture Toughness*. Weld. Inst. and ASM, London (1976).
15. G. C. Angelino, Influence of the geometry on unstable crack extension and determination of dynamic fracture mechanics parameters. ASTM STP No. 627, ASTM (1977).
16. B. Brickstad and F. Nilsson, Numerical evaluation of FEM of crack propagation experiments. *Int. J. Fracture* **16**, 71 (1980).
17. N. F. Mott, Brittle fracture in mild-steel plates. *Engineering* **165**, 16 (1948).
18. D. K. Roberts and A. A. Wells, The velocity of brittle fracture. *Engineering* **178**, 820 (1954).
19. K. B. Broberg, The propagation of a brittle crack. *Arkiv fur Fysik* **18**, 159 (1960).
20. E. H. Yoffe, The moving Griffith crack. *Phil. Mag.* **42**, 739 (1951).
21. J. W. Craggs, On the propagation of a crack in an elastic-brittle material. *J. Mech. Phys. Solids* **8**, 66 (1960).
22. H. Bergkvist, The motion of a brittle crack. *J. Mech. Phys. Solids* **21**, 299 (1973).
23. B. Cottrell, Velocity effects in fracture propagation. *Appl. Math. Res.* **4**, 227 (1965).
24. K. B. Broberg, On the speed of a brittle crack. *J. Appl. Mech.* **31**, 546 (1964).
25. L. B. Freund, Crack propagation in an elastic solid subjected to general loading; I—Constant rate of extension. *J. Mech. Phys. Solids* **20**, 129 (1972); II—Nonuniform rate extension. *J. Mech. Phys. Solids* **20**, 141 (1972).
26. L. B. Freund, Dynamic crack propagation. *Mech. Fracture AMD* **19**, 105 (1976).
27. L. R. F. Rose, Recent theoretical and experimental results on fast brittle fracture. *Int. J. Fracture* **12**, 799 (1976).
28. B. V. Kostrov, Crack propagation at variable velocity. *Int. J. Fracture* **11**, 47 (1975).
29. K. B. Broberg, On the behavior of the process region at a fast running crack. *Proc. IUTAM Symp. Tokyo* 1977, Springer, Berlin (1977).
30. J. Klepaczko, An experimental method in ductile crack propagation dynamics for some aluminum alloys. *Problemes Non-linearies de Mechanique*. Polish Scientific Publishers, Warsaw (1980).
31. J. D. Campbell and W. G. Ferguson, The temperature and strain-rate dependence of the shear strength of mild steel. *Phil. Mag.* **21**, 63 (1970).
32. G. M. McClure, A. R. Duffy and R. J. Eiber, Fracture resistance in line pipe. *J. Engng for Industry* **87**, 265 (1965).
33. A. R. Duffy, G. M. McClure, R. J. Eiber and W. A. Maxey, Fracture design practices for pressure piping. *Fracture* (Edited by H. Liebowitz), Vol. 5. Academic Press, New York (1969).
34. R. M. Davies, A critical study of the Hopkinson pressure bar. *Phil. Trans.* **A240**, 375 (1948).
35. H. Kolsky, *Stress Waves in Solids*. Dover, New York (1963).
36. G. T. Hahn, R. G. Hoagland, M. F. Kanninen and A. R. Rosenfield, A preliminary study of fast fracture and arrest in the DCB test specimen. *Dynamic Crack Propagation* (Edited by G. C. Sih). Noordhoff, Leyden (1973).
37. Z. J. Bilek and S. J. Burns, Crack propagation in wedged double cantilevered beam specimen. *J. Mech. Phys. Solids* **22**, 85 (1974).
38. R. Dormeval, J. M. Chevallier and M. Stelly, Fracture initiation of metals at high loading rates. *Proc. Fifth Int. Conf. on Fracture*, Cannes (1981).
39. J. W. Phillips, Stress pulses produced during the fracture of brittle tensile specimens. *Int. J. Solids Struct.* **6**, 1403 (1970).
40. H. Kolsky, The stress pulses propagated as a result of the rapid growth of brittle fracture. *Engng Fracture Mech.* **5**, 513 (1973).
41. K. Oi, Transient response of bonded strain gages. *Exp. Mech.* **6**, 463 (1966).
42. J. Miklowitz, Elastic waves created during tensile fracture. *J. Appl. Mech.* **20**, 122 (1952).
43. J. M. Krafft, Test for fracture strength, static to impact. *Measurement of Mechanical Properties* (Edited by R. F. Burshah), Chap. 7. Interscience, New York (1971).
44. P. Lipiński, Stress concentration and crack dynamics in notched bars. Ph.D. Thesis, Institute of Fundamental Technological Research, Warsaw (1979).